ELSEVIER

Thermochimica Acta 360 (2000) 131–140

thermochimica acta

www.elsevier.com/locate/tca

Study of temperature profile and specific heat capacity in temperature modulated DSC with a low sample heat diffusivity

S.X. Xu[a,*], Y. Li[a], Y.P. Feng[b]

[a]*Department of Materials Science, Faculty of Science, National University of Singapore, Lower Kent Ridge Road, Singapore, Singapore*
[b]*Department of Physics, National University of Singapore, Singapore, Singapore*

Received 12 December 1999; received in revised form 25 March 2000; accepted 21 May 2000

Abstract

One important application of temperature modulated DSC (TMDSC) is the measurement of specific heat of materials. When the sample has very good thermal conductivity as in the case of metals, the temperature gradient is not normally an important factor and can be ignored most of the time. However, in the case of materials with poor heat transfer properties, for example, polymers, the thermal conductivity is only in the order of 1/1000 or so of that of metals. This could have a major effect on the test results. In this paper, a round analytical solution is given and a numerical model is used to analyze the effects of thermal diffusivity on temperature distribution inside the test sample and specific heat measurement by TMDSC, PET sample test results are presented to demonstrate the effects of material thermal diffusivity.

Keywords: TMDSC; Specific heat; Thermal diffusivity; Temperature gradient

1. Introduction

Temperature modulated differential scanning calorimetry (TMDSC), which was first introduced by Reading and coworkers in 1992 [1], became commercialized shortly afterwards and is being widely applied to materials research including polymer, food, pharmaceutical and metallic materials. TMDSC, where normally a sinusoidal temperature signal is superimposed onto a linear underlying heating rate, can be used to measure material thermal properties, such as specific heat. Specific heat measurement under isothermal conditions that has a zero underlying heating rate with TMDSC was also reported [2,3].

In a heat flux type DSC cell, if the temperature gradient inside the sample is negligible, we have the following heat transfer equation on the reference side,

$$\mathrm{HF_s} = C_\mathrm{s}\frac{\mathrm{d}T_\mathrm{s}}{\mathrm{d}t} = K(T_\mathrm{b} - T_\mathrm{s}) \tag{1}$$

where T_b is the heating block temperature, T_s sample temperature, $C_\mathrm{s}(=C_\mathrm{s}'+C_\mathrm{r})$ sample side total heat capacity, C_s' the sample's heat capacity, C_r the heat capacity of the reference or sample container (assuming the reference is the same as the sample container), K is system heat transfer coefficient.

On the reference side, the heat flow $\mathrm{HF_r}$ to the reference, which is typically an empty container same as that used to seal the sample is

$$\mathrm{HF_r} = C_\mathrm{r}\frac{\mathrm{d}T_\mathrm{r}}{\mathrm{d}t} = K(T_\mathrm{b} - T_\mathrm{r}) \tag{2}$$

where T_r is the reference temperature.

* Corresponding author.
E-mail address: scip7317@nus.edu.sg (S.X. Xu).

0040-6031/00/$ – see front matter
PII: S0040-6031(00)00564-5

In temperature modulated DSC, the sample heat capacity can be obtained by [2]:

$$C'_s = \frac{A_{\Delta T}}{A_{T_s}} \sqrt{\left(\frac{K}{\omega}\right)^2 + C_r^2} \tag{3}$$

where $A_{\Delta T}$ is the amplitude of the reference-sample temperature difference, A_{T_s} is the sample temperature amplitude and ω is the modulation temperature frequency.

It has been noticed that the measured sample specific heat drops when the sample size reaches a certain value, and the reason is attributed to insufficient heat diffusion in the sample [2]. Efforts were also made in analyzing the sample temperature profile in both conventional DSC and TMDSC. It was found that poor sample thermal conductivity can lead to an increased phase lag [4–6] which may cause incorrect interpretation of certain experimental results, such as the physical meaning of the in phase and out of phase part of the measured heat flow and complex heat capacity [7–9]. Generally, for metallic materials, the heat conducting capabilities are good and the temperature distribution is almost uniform through out the sample. In this case, heat diffusivity has very little effect on the observed specific heat. However, for materials that have very low heat diffusivity, the extra thermal resistance introduced by the sample itself can significantly affect the observed specific heat value. PET, which has a thermal conductivity only about one thousandth that of aluminum, is used as an example in our study.

2. TMDSC model with thermal diffusivity in consideration

Fig. 1 shows the simplified heat flux type TMDSC cell structure. The sample material is PET, where the C_r is the heat capacity of the support plate (the support plate itself is used as the reference in this model), K system heat transfer coefficient, T_r is the reference side thermocouple temperature, T_s is the sample side thermal couple temperature. It should be pointed out that the sample temperature can not be measured directly in DSC or TMDSC. Instead, the thermocouple temperature is used to evaluate the sample heat capacity. For the sake of simplicity, the sample is assumed to be heated only on the bottom surface, top and side surfaces have no heat exchange with the environment either by convection or by radiation, and there is no heat exchange between sample and reference support plate.

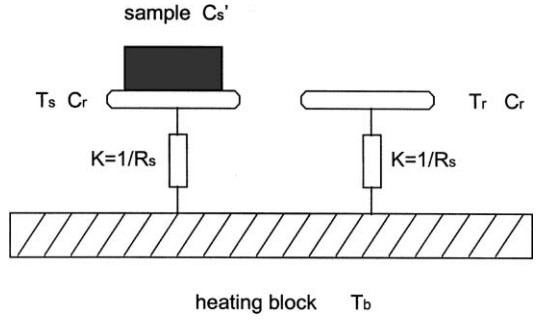

Fig. 1. Simplified DSC/MDSC cell with the temperature gradient in consideration, in the calculation, the cylindrical PET sample is equally divided into 10 small disks along its axis for finite element calculation. T_r is the reference temperature, T_s the measured sample temperature (or thermal couple temperature), C_r the heat capacity of the support plate, $K=1/R_s$ is the system thermal constant.

2.1. Analytical solution to the model

Based on the above assumptions, we can treat the sample as an ideal one dimensional heat transfer problem. The sample will follow the general heat transfer equation,

$$\frac{\partial T(x,t)}{\partial t}\frac{1}{\alpha} = \frac{\partial^2 T(x,t)}{\partial x^2} \tag{4}$$

where thermal diffusivity $\alpha=\lambda/(\rho c_p)$, λ is thermal conductivity, ρ sample density, c_p specific heat, x the distance from the sample bottom.

Assuming the thermal couple temperature on the sample side (same as the sample bottom surface temperature if we ignore the temperature gradient inside the metallic support plate and assume the contact between the sample and the support plate is perfect) is modulated in a sinusoidal pattern,

$$T_s = T_s(0,t) = A \times e^{i\omega t} \tag{5}$$

where T_0 is the initial temperature, A amplitude, ω modulation angular frequency. The oscillating part of the solution to Eq. (4) can take the form

$$T_s(x,t) = F(x) \times e^{i\omega t} \tag{6}$$

it can be shown that [10]:

$$F(x) = A_1 e^{-x(1+i)\sqrt{\omega/2\alpha}} + A_2 e^{x(1+i)\sqrt{\omega/2\alpha}} \quad (7)$$

By utilizing the boundary conditions, $F(0)=A$, and $\partial T(x,t)/\partial x|_{x=d}=0$, d is sample thickness (because there is no heat flow through the top surface in this model) one can obtain,

$$A_2 = \frac{e^{-\beta d}}{e^{\beta d} + e^{-\beta d}} \quad (8a)$$

$$A_1 = \frac{e^{\beta d}}{e^{\beta d} + e^{-\beta d}} \quad (8b)$$

in the above equations,

$$\beta = (1+i)\sqrt{\frac{\omega}{2\alpha}} \quad (9)$$

Thus, the oscillation part of the sample temperature is

$$T_s(x,t) = \frac{1}{e^{\beta d} + e^{-\beta d}} (e^{\beta d} e^{-\beta x} + e^{-\beta d} e^{\beta x}) A \times e^{i\omega t} \quad (10)$$

In this case, the left hand side of Eq. (1) is the heat absorbed by the support plate and the sample with temperature gradient in consideration, hence it can be obtained that,

$$K(T_b - T_s(0,t)) = C_r \frac{dT_s(0,t)}{dt} + \int_0^d \left(S \times c_p \rho \frac{\partial T_s(x,t)}{\partial t} \right) dx \quad (11)$$

where S is the sample cross section area, and hence,

$$T_b = \frac{1}{K} \left(K \times T_s(0,t) + C_r \frac{dT_s(0,t)}{dt} + \int_0^d \left(S \times c_p \rho \frac{\partial T_s(x,t)}{\partial t} \right) dx \right) = \frac{1}{K} \times A \times e^{i\omega t} \times \left(K + i\omega \times C_r + i\omega \times S \times c_p \rho \frac{1}{\beta} \frac{e^{\beta d} - e^{-\beta d}}{e^{\beta d} + e^{-\beta d}} \right) \quad (12)$$

Inserting Eq. (12) into Eq. (2), one gets the cyclic part of the reference side temperature T_r as,

$$T_r = A \times e^{i\omega t} \left(K + i\omega \times C_r + i\omega \times S \times c_p \rho \frac{1}{\beta} \frac{e^{\beta d} - e^{-\beta d}}{e^{\beta d} + e^{-\beta d}} \right) \frac{1}{i\omega \times C_r + K} \quad (13)$$

Inserting the Eqs. (13) and (5) into Eq. (3), one gets the measured sample heat capacity as,

$$C_s' = \left(\frac{K + i\omega \times C_r + i\omega \times S \times c_p \rho (1/\beta)\{(e^{\beta d} - e^{-\beta d})/(e^{\beta d} + e^{-\beta d})\}}{i\omega \times C_r + K} - 1 \right) \sqrt{\left(\frac{K}{\omega}\right)^2 + C_r^2} = \left(\frac{e^{2\beta d} - 1}{e^{2\beta d} + 1} \frac{1}{\beta} \frac{i\omega \times S \times c_p \rho}{i\omega \times C_r + K} \right) \sqrt{\left(\frac{K}{\omega}\right)^2 + C_r^2} \quad (14)$$

Given the above, let us now consider the effects of the variables under certain extreme situations.

1. Sample thermal conductivity. When the sample's heat conductivity is extremely large, i.e. $\lambda \to \infty$, thus, its thermal diffusivity $\alpha = \lambda/(\rho c_p) \to \infty$. Then per definition in Eq. (9), $\beta \to 0$.

   This is the original ideal model where it was assumed there is no temperature gradient inside the sample, the following part in Eq. (14) will obey,

$$\lim_{\beta \to 0} \frac{e^{2\beta d} - 1}{e^{2\beta d} + 1} \frac{1}{\beta} = \lim_{\beta \to 0} \frac{e^{2\beta d} - 1}{2\beta} = \lim_{\beta \to 0} \frac{2d \times e^{2\beta d}}{2} = d \quad (15)$$

   Then it can be dereived from Eq. (14) together with Eq. (15) that

$$\lim_{\beta \to 0} \left| \left(\frac{e^{2\beta d} - 1}{e^{2\beta d} + 1} \frac{1}{\beta} \frac{i\omega \times S \times c_p \rho}{i\omega \times C_r + K} \right) \sqrt{\left(\frac{K}{\omega}\right)^2 + C_r^2} \right| = d \times S \times c_p \rho \quad (16)$$

   The right hand side is the sample's real heat capacity, hence the well established expression is obtained again.

   One the other extreme end, the thermal conductivity is very poor, $\lambda \to 0$, then we have $\beta \to \infty$, hence it will follow that,

$$\lim_{\beta \to \infty} \left| \frac{e^{2\beta d} - 1}{e^{2\beta d} + 1} \cdot \frac{1}{\beta} \right| = 0 \quad (17)$$

which means the measured heat capacoty will be very low in this case.

2. Sample thickness. When the sample thichness is very thick, $d\to\infty$, we can obtain that,

$$\lim_{d\to\infty}\frac{\left|\{(e^{2\beta d}-1)/(e^{2\beta d}+1)\}(1/\beta)\{(i\omega\times S\times c_p\rho)/(i\omega\times C_r+K)\}\sqrt{(K/\omega)^2+C_r^2}\right|}{d\times S\times c_p\rho}$$
$$=\lim_{d\to\infty}\left|\frac{e^{2\beta d}-1}{e^{2\beta d}+1}\cdot\frac{1}{d\times\beta}\right|=0 \quad (18)$$

As can be seen, the measured sample heat capacity will be very low when compared with its real heat capacity.

On the contrary, if a very thin sample is used, $d\to0$, it is easy to get (silmilar to Eq. (18)),

$$\lim_{d\to0}\left|\frac{e^{2\beta d}-1}{e^{2\beta d}+1}\frac{1}{d\times\beta}\right|=\lim_{d\to0}\left|\frac{e^{2\beta d}-1}{2}\frac{1}{d\times\beta}\right|$$
$$=\lim_{d\to0}\left|\frac{2\beta\times e^{2\beta d}}{2}\frac{1}{\beta}\right|=1 \quad (19)$$

hence obviously, measured sample heat capacity should be more accuate for thin samples.

3. Modulation frequency. For a very slow temeprature modulation frequency, $\omega\to0$, thus, $\beta\to0$ per Eq. (9). By re-arranging the left hand side of Eq. (16), we get,

$$\lim_{\omega\to0}\left|\left(\frac{e^{2\beta d}-1}{e^{2\beta d}+1}\frac{1}{\beta}\frac{i\omega\times S\times c_p\rho}{i\omega\times C_r+K}\right)\sqrt{\left(\frac{K}{\omega}\right)^2+C_r}\right|$$
$$=\lim_{\omega\to0}\left|\left(\frac{e^{2\beta d}-1}{e^{2\beta d}+1}\frac{1}{\beta}\frac{iS\times c_p\rho}{i\omega\times C_r+K}\right)\sqrt{K^2+(\omega\times C_r)^2}\right|$$
$$=\lim_{\omega\to0}\left|\left(\frac{e^{2\beta d}-1}{e^{2\beta d}+1}\frac{1}{\beta}\right)\right|S\times c_p\rho$$
$$=\lim_{\beta\to0}\left|\left(\frac{e^{2\beta d}-1}{e^{2\beta d}+1}\frac{1}{\beta}\right)\right|S\times c_p\rho=d\times S\times c_p\rho \quad (20)$$

which means we should be able to get very accurate heat capacity results with a very long modulation period theoretically. (In real practice, with too long a modulaiton period, say, 2000 s, the spectrum of heat flow signal may overlap with instrument background noise or slow drifting et. al. The final signal/noise ratio may not be as good as a moderately chosen one.) By the same deriviation as in Eq. (20), it can be obtained the measured sample heat capacity will be zero if the modulation frequency is infinitely fast ($\omega\to\infty$). In short, thin samples with high coductivity, and low modulation frequencies will be benifitial to improving the test accuracy of TMDSC.

As shown above, a slight increase in the model complexity can drastically increase the difficulty of deriving a round analytical solution and in many cases the process can be very difficult if not impossible. Sometimes the effect of each variable may not be so obvious but deeply buried inside the cumbersome equations.

2.2. Numerical approach to the problem

For the purpose of comparison, we now resort to a numerical approach again. The cylindrical sample is divided into a number of equally sized small disks along its vertical axis. From the above model, the following heat transfer differential equations can be obtained,

sample support:

$$(T_b-T_s)K-(T_s-T_1)/R_{unit}=C_r\frac{dT_s}{dt} \quad (21)$$

sample unit 1 (at the sample bottom):

$$\frac{(T_s-2T_1+T_2)}{R_{unit}}=C_{unit}\frac{dT_1}{dt} \quad (22)$$

sample unit i=2 to (n−1) (small units in between):

$$\frac{(T_{i-1}-2T_i+T_{i+1})}{R_{unit}}=C_{unit}\frac{dT_i}{dt} \quad (23)$$

sample unit n (unit on the sample top, n=10):

$$\frac{(T_{n-1}-T_n)}{R_{unit}}=C_{unit}\frac{dT_n}{dt} \quad (24)$$

where R_{unit} is the thermal resistance of each small unit disk, C_{unit} is the heat capacity of the small sample unit, T_i the temperature of the ith sample unit disk.

Table 1
Simulation parameters associated with the modelling approach

Reference heat capacity C_r (J/K)	0.02
PET sample density (g/cm^3)	1.37 [11]
PET sample diameter (mm)	5
PET sample size (g)	0.02
PET sample specific heat (J/g K)	1.25 [11]
PET thermal conductivity (W/m K)	0.0029 [11]
TMDSC system heat transfer coefficient K (W/K)	0.01

reference support:

$$(T_b - T_r)K = C_r \frac{dT}{dt} \quad (25)$$

Simulation conditions are listed in Table 1. DSC simulation is carried out to obtain the sample temperature profile under different linear heating rate, while TMDSC simulation is used to find out the effect of sample heat conductivity on the measured specific heat under quasi-isothermal heating conditions. Finite difference method and discrete Fourier transfer are used to calculate the measured sample heat capacity per Eq. (3).

3. Experimental

In the conventional DSC experiment to study the temperature difference inside the PET sample, small amount of indium was used as a temperature tracer, as shown in Fig. 2, the PET sheet thickness is 0.4 mm, a very small quantity of indium (with a mass in the order of 10^{-2}–10^{-1} mg) is sandwiched between two PET sheets and at the bottom position, then the sample is sealed with a standard aluminum pan. Upon linear heating, when the temperature reaches the melting point of indium, the embedded indium will melt and a signal will be picked up by the thermal couple underneath. The amount of indium should be very small so that it will affect the PET temperature distribution as little as possible. Due to the temperature gradient inside PET, two indium melting peaks will be detected during the linear temperature scan. From the measured peak temperature difference, we can roughly deduce the temperature profile in the sample. The observed temperature difference between the two small indium melting peaks should be corrected with the heat diffusion time delay, since the signal from the indium in the middle position will take longer to arrive at the thermal couple. For a PET sample, the heat diffusivity D is 0.093×10^{-6} m^2/s [12]. Given a sample thickness of 0.4 mm, it will produce a time delay of $(0.4\times10^{-3})^2/D$=1.7 s. Thus, this can make another temperature difference of $1.7q$, where q is the DSC linear heating rate. Hence this extra difference should be deducted from the above measured values. The linear scanning rate used in our DSC experiment changes from 2 to 40 K/min.

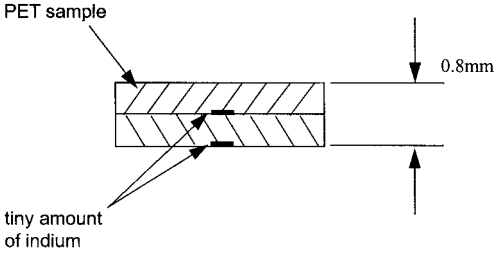

Fig. 2. PET sample used in the conventional DSC experiments, tiny amount of indium is embedded in the middle and at bottom positions. The sample is then sealed with a standard aluminum pan.

In the TMDSC experiments, two PET samples with a mass of 6.71 mg (single layer of sheet, 0.4 mm thick) and 19.6 mg (double layers of sheet, 0.8 mm thick), respectively, without embedded indium is used. The temperature modulation amplitude is 0.5–2 K, modulation period varies from 10 to 100 s. Quasi-isothermal temperature is 160°C. A standard sapphire disk with a mass of 18.25 mg is used as the calibration material and calibration is conducted at each modulation period experienced by the PET sample.

All DSC/TMDSC experiments are carried out on a TA 2920 DSC/MDSC thermal analysis instrument, equipped with a rapid cooling system, and nitrogen is used as the cell purge gas at a flow rate of 70 cc/min.

4. Results and discussion

The conventional DSC heat flow curves obtained with PET samples embedded with tiny amount of indium are given in Fig. 3. In each curve, it is quite clear that there are two heat flow peaks corresponding to the melting of the embedded indium in the middle and at the bottom positions. Fig. 4 shows the comparison between the DSC experimental temperature

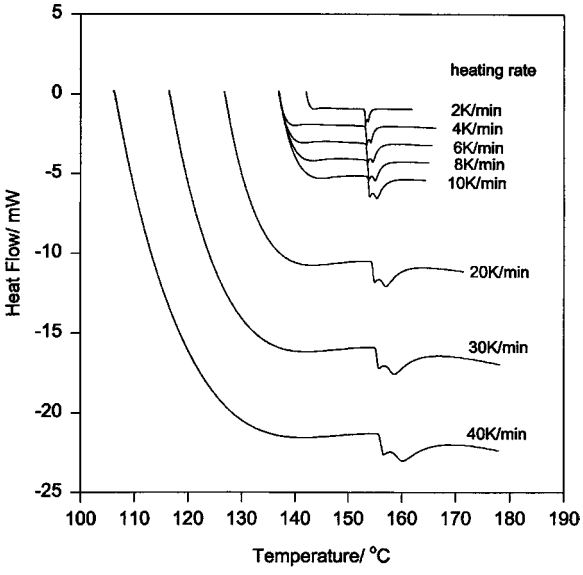

Fig. 3. Heat flow curves of a PET sample embedded with indium under different heating rate.

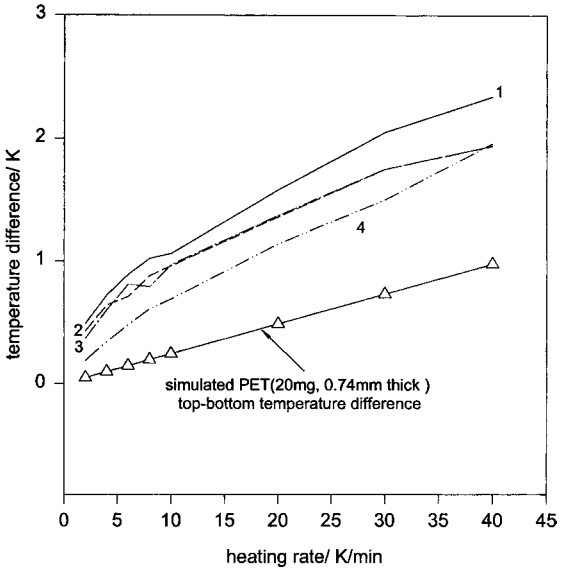

Fig. 4. Curves 1–4 are experimentally measured temperature difference, while the straight line is that obtained from numerical simulation. Curve 1, PET size 14.24 mg, middle/bottom indium mass are 0.43/0.38 mg, respectively; curve 2, PET size 13.02 mg, middle/bottom indium mass are 0.27/0.23 mg, respectively; curve 3, PET size 12.94 mg, middle/bottom indium mass are 0.17/0.12 mg, respectively; curve 4, PET size 18.17 mg, middle/bottom indium mass are 0.69/0.07 mg, respectively.

difference after the time delay in indium melting have been taken into account and that of the simulated result. As can be seen, all the four experimental curves basically exhibit a linear relationship to the heating rate. The embedded indium mass in the four PET samples varies from 0.06 to 0.69 mg, but there seems to be no specific pattern between the indium size and the temperature difference. Thus, the curve values should approximately reflect the real situation. It can be noted that in the simulation, the PET sample mass is 20 mg and is assumed to have a perfect contact with the support plate. Based on the density and diameter given in Table 1, it has a thickness of 0.74 mm, while in the experimental samples the mid/bottom distance is only 0.4 mm, as indicated in Fig. 2. However, the measured mid/bottom temperature difference is higher than the simulated top/bottom temperature difference. This should be caused by the non-ideal heat transfer conditions (through purge gas, radiation and less than perfect or partial thermal contact between the PET sample and the aluminum sealing pan).

Fig. 5 gives the simulated relative temperature distribution inside the PET sample as a function of depth and heating rate after heating for one minute in DSC simulation, which is enough for the sample temperature distribution to get into a quasi-steady

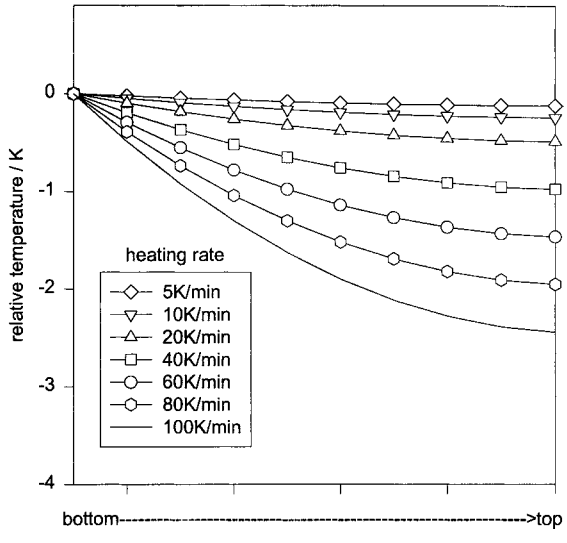

Fig. 5. Sample relative temperature distribution as a function of heating rate in conventional DSC by simulation. Sample bottom temperature is the reference point and set to zero.

state. In this figure, the bottom temperature is the reference point and set to be zero. It can be noticed that although the temperature distribution curve itself is not a straight line, the temperature difference between any two points inside the sample is proportional to the heating rate. When the heating rate is 100 K/min, a temperature difference of 2.4 K will develop between the top and bottom surface.

For TMDSC, in Fig. 6 we can see the simulated temperature oscillation amplitude inside the sample vs. different modulation period. In the simulation, the 20 mg PET sample has a thermal resistance of 130 K/W, which is even bigger than that of the cell itself (R_s=100 K/W). This extra thermal resistance changes the effective system constant K and puts the TMDSC cell into a biased (or asymmetric) state. While the heat capacity calibration material does not have such a big resistance, it can be expected that deviations can be produced if the calibration factor obtained from the later is used to correct the measured heat capacity or specific heat of the PET sample. Apparently, as the PET sample gets thinner, its temperature will also be more evenly distributed hence the more accurate the test results. Heat diffusion into the sample is quite limited at short modulation periods, such as 5–20 s.

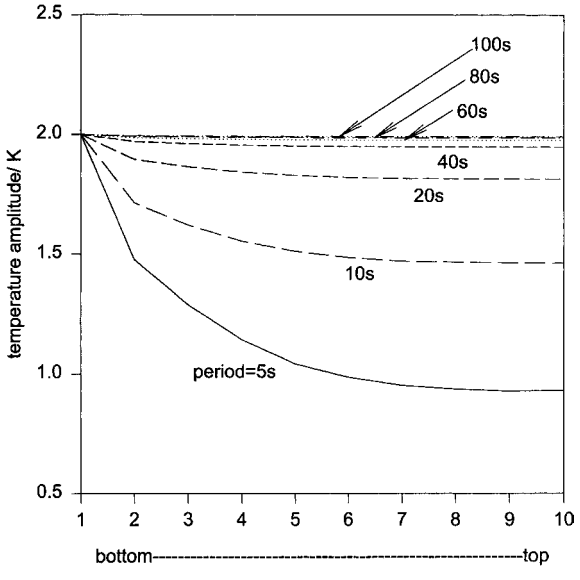

Fig. 6. Simulated temperature oscillation amplitude as a function of modulation period in TMDSC. Programmed (or the sample bottom) modulation amplitude is 2 K; 20 mg PET.

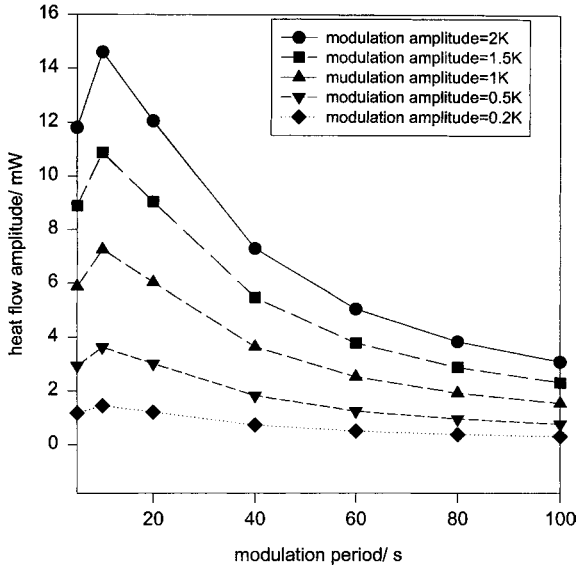

Fig. 7. Simulated heat flow amplitude as a function of modulation period and amplitude in TMDSC; 20 mg PET.

Due to the obvious dampening effect, except at the sample bottom surface, the amplitude profile of temperature oscillation can not quite follow the modulation and is far below the programmed 2 K amplitude as it goes deep into the sample. When the modulation period increases, the amplitude profile gets closer to the programmed value and exhibits a more flat pattern.

Fig. 7 shows the simulated heat flow amplitude curves against the modulation period. In this figure, the simulated heat flow amplitude curves exhibit an increasing tendency as modulation period increases, a maximum point is reached at about 10 s and then decreases with period. Compared with that of the experimentally measured curves in Fig. 8, this trend is similar except that in the experiment, the amplitude curves show a maximum at different modulation period. As can be seen in Fig. 8, when the modulation temperature amplitude is 0.5 K, the maximum appears at a period of 30 s, but when the temperature modulation is 2 K, it occurs at about 45 s. This peak shift could be attributed to the much more complicated TMDSC cell heat transfer properties than the simple model for the simulation. Fig. 9 is the experimentally determined relationship between sample modulation amplitude and modulation period. It demonstrates the maximum cooling heating capabilities of the system,

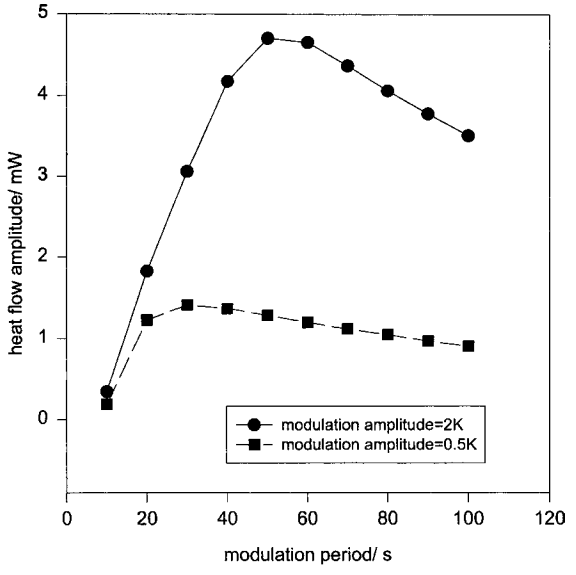

Fig. 8. Experimentally determined heat flow amplitude in TMDSC; 19.6 mg PET.

i.e. an amplitude of 0.5 K can be reached when the modulation period gets 20 s and above, while an amplitude of 2 K needs a period of 60 s or more, but this limitation does not exist in the idealized model.

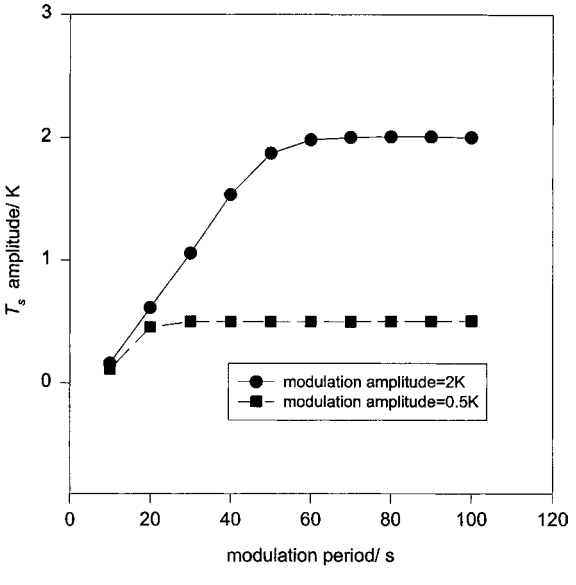

Fig. 9. Experimentally determined T_s amplitude as a function of modulation period and amplitude.

With a sinusoidal temperature modulation, the instant maximum heating rate for quasi-isothermal TMDSC is $A\omega$ (A is the programmed modulation amplitude, ω the modulation frequency), which is proportional to the modulation temperature amplitude and angular frequency. This will give a maximum instant heating rate ranging from 7.5 to 75 K/min for a modulation temperature amplitude of 2 K and from 1.9 to 19 K/min for 0.5 K amplitude when the modulation period falls between 10 and 100 s. By referring to the measured conventional DSC curves in Fig. 4, it is believed the modulation can produce a temperature difference in the order of 10^{-1}–1° inside the sample. Although this may not seem too big by its absolute value, the ratio to the modulation temperature amplitude is not negligible which can cause significant error in specific heat capacity measurement. Interesting enough, simulation shows there is a linear relationship between modulation temperature amplitudes and heat flow/the internal temperature amplitude of the sample, which means for a given sample and modulation period, the test error is fixed regardless of the modulation amplitude. This can be explained by the characteristics of the linear differential equations used in the model. Computer simulated effect of sample mass (or thickness) on the obtained specific heat capacity is shown in Fig. 10. While the 20 mg PET sample deviates a lot from the real value, especially at higher modulation frequencies, the situation gets much better for the 5 mg one. As a matter of fact, in dynamic temperature differential scanning calorimetry, although the detailed algorithms and implementations are different, these results agree well with those obtained for a power compensated DSC, DDSC and SSADSC, either by analytical or numerical approaches, except that one method may be more accurate than another [13–15].

Experimental results are given in Fig. 11, where the programmed modulation amplitude increased from 0.5 to 2 K, the obtained c_p does not exhibit significant change when compared with that of the modulation period. The relationship between sample mass (thickness) and observed c_p agrees well with computer simulation. For the 6.71 mg sample, its c_p curve pattern is much better than the 19.6 mg one, however, when period gets smaller than 10–20 s, the curve value increases with shorter period. This may be explained by the contact resistance that begins to play a more

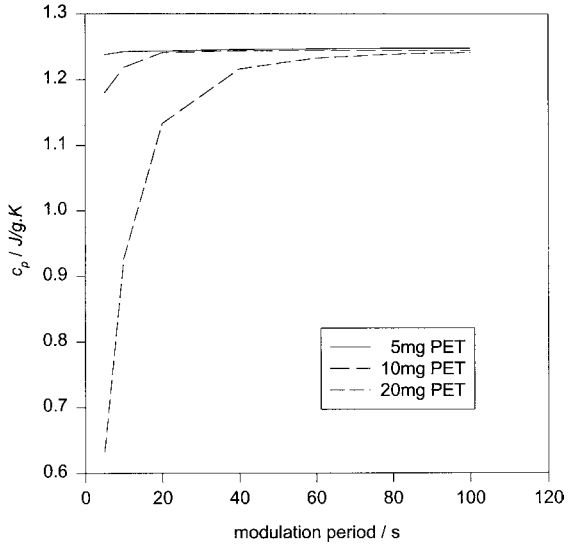

Fig. 10. 'Measured' specific heat as a function of modulation period by computer simulation. In the simulation, the 5, 10 and 20 mg PET samples have the same foot print, thus, the smaller the mass the thinner the sample.

important role at the higher frequency region, which is the subject of another paper [16]. Apparently, in our experiments, the 19.6 mg PET sample appears to be too thick for such a heat capacity test, because it seems

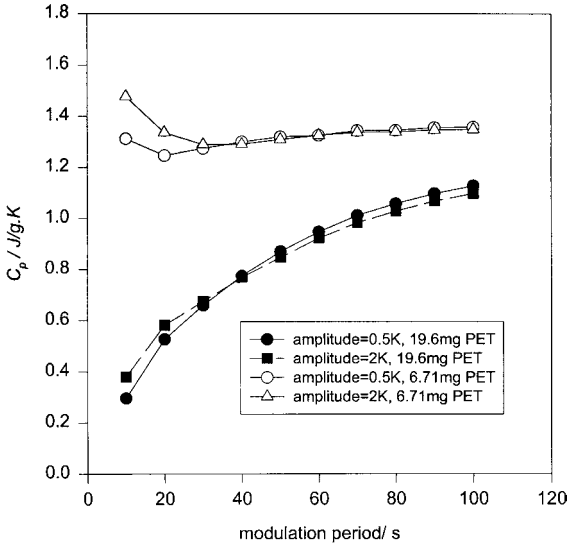

Fig. 11. Experimentally determined specific heat capacity as a function of modulation period. The thickness of the 6.71 mg sample is 0.4 mg, while the thickness of the 19.6 mg sample is 0.8 mg (double layer of PET sheet) with a bigger footprint.

a modulation period much longer than the upper limit of 100 s is needed for its c_p curve to get into stable stage.

5. Conclusions

The effect of sample heat diffusivity can usually be ignored for metal samples in differential calorimetry. However, this is not always the case for materials with very poor heat conducting abilities. In this paper, an analytical is given. Simulation and experiments with PET samples are conducted and several factors have been identified.

When testing heat capacity test for poor heat conductors, sample thickness should be minimized for low thermal conducting materials. As the extra thermal resistance from the above two sources will decrease the effective system constant K, which is not experienced by the calibration material that has a much higher heat diffusivity, the measured specific heat capacity even after calibration will still deviate from the actual value. Also the modulation period should be in the high side of available range of the instrument. While the fact that modulation amplitude has relatively small effect on the test results is a good indication of the overall system linearity of the TMDSC test facilities, especially at large modulation periods that is well within its cooling/heating capability.

References

[1] S.R. Sauerbrunn, B.S. Crow, M. Reading, in: Proceedings of the 21st NATAS Conference, Atlanta, GA, USA, 13–16 September 1992.
[2] A. Boller, Y. Jin, B. Wunderlich, J. Therm. Anal. 42 (1994) 307.
[3] B. Wunderlich, Y. Jin, A. Boller, Thermochim. Acta 238 (1994) 277.
[4] Z. Jiang, T. Corrie, J. Imrie, M. Huchinson, Thermochim. Acta 315 (1998) 1–9.
[5] Z. Jiang, T. Corrie, J. Imrie, M. Huchinson, Thermochim. Acta 336 (1999) 27–40.
[6] S. Weyer, A. Hensel, C. Schick, Thermochim. Acta 305 (1997) 267–275.
[7] P. Skoglund, A. Fransson, Thermochim. Acta 276 (1996) 27–39.
[8] F.U. Buehler, J.C. Seferis, Thermochim. Acta 334 (1999) 49–55.

[9] F.U. Buehler, C.J. Martin, J.C. Seferis, J. Therm. Anal. 54 (1998) 501.
[10] S. Kakac, Y. Yener, Heat Conduction, 3rd Edition, Hemisphere Pub. Corp., Washington, 1985, p. 215.
[11] Igor S. Grigoriev, Evgenii Z. Meilikhov, Handbook of Physical Quantities, CRC Press, Boca Raton, 1977.
[12] J. Brandrup, E.H. Emergut, Polymer Handbook, 2nd Edition, Wiley, New York, 1975.
[13] M. Merzlyakov, C. Schick, Thermochim. Acta 330 (1999) 65–73.
[14] B. Schenker, F. Stager, Thermochim. Acta 304/305 (1997) 219–228.
[15] En-Yong Ding, Rong-Shi Cheng, Yu-Hui Huang, Thermochim. Acta 336 (1999) 1–15.
[16] S.X. Xu, Y. Li, Y.P. Feng, Thermochim. Acta, submitted for publication.